

Study on Multi-flow Field Characteristics of Unloading Groove Spacing of Bidirectional Gear Pump

H. Zhang[†], D. Y. Zhan, R. Q. Tian and T. A. Zhang

School of Mechanical Engineering, Dalian University of Technology, Dalian, Liaoning Province, 116024, China

[†]Corresponding Author Email: 22004051@mail.dlut.edu.cn

(Received October 2, 2022; accepted January 19, 2023)

ABSTRACT

Improving the output flow quality of the high-precision micro bidirectional gear pump can effectively improve the position control accuracy and dynamic characteristics of the electro-hydraulic actuator. In order to meet the appeal requirements and reduce the vibration and noise of the gear pump and prolong its working life, this paper starts with the research of the key part of the gear pump—the unloading groove structure. The three characteristics of trapped oil phenomenon, cavitation phenomenon, and flow were used as key indices to evaluate gear pump performance. Using numerical simulation analysis, the dynamic grid simulation method was used to explore the influence of unloading groove spacing on the transient multi-flow field characteristics of the gear pump under conventional design range. Our results show that reducing the distance between unloading grooves can greatly reduce the trapped oil pressure and the amount of gas precipitation in the flow field, while reducing flow pulsation and improving volumetric efficiency. However, when the unloading groove spacing is too small, the instantaneous flow curve loses the pulsation characteristics and the flow stability decreases. Considering the influence of the gear pump on the accuracy of the electro-hydraulic actuator and the performance of the gear pump itself, the analytic hierarchy process was used to obtain the 1 mm unloading slot spacing, which best meets the engineering requirements of high flow accuracy and low vibration noise. The results provide a basis for work on the structural optimization of high-precision micro gear pumps.

Keywords: Bidirectional gear pump; Unloading groove spacing; Numerical simulation; Dynamic mesh; Flow field characteristics.

NOMENCLATURE

B	tooth thickness	R_c	bubble collapse rate
d_a	addendum circle diameter	R_e	bubble generation rate
d_f	root circle diameter	t	time
d_o	outlet diameter	t_j	gear base pitch
F	local uniformity	T	maximum gas volume fraction
h_a	axial clearance	x_i	displacement of node i
h_r	radial clearance	x_j	displacement of node j
i	node	Y	evaluating indicator
k_{ij}	spring stiffness between nodes	z	tooth number
L	node connection length	α	pressure angle
m	modulus	δ	flow pulsation coefficient
n	number of connected nodes	λ	latent root
P	maximum trapped oil pressure	ρ_v	density of gas phase
Q_a	average flow	φ_g	gas volume fraction
r_a	addendum circle radius	ω	angular velocity
r_k	pitch radius		

1. INTRODUCTION

For the closed electro-hydraulic actuator with high

control precision and high automation in the power industry, the performance of the power unit as the core link determines the flow pulsation, output efficiency and positioning accuracy of the hydraulic

cylinder piston rod of the actuator to a large extent. Because the hydraulic components in the closed electro-hydraulic actuator need to be immersed in oil for a long time in the working state, and the actuator has restrictions on the structural size of the hydraulic system, and it is required to meet the working conditions of bidirectional oil supply, micro-flow transportation, fixed displacement supply and low noise. Therefore, a high-precision bidirectional gear pump with low oil sensitivity, small volume, small displacement, simple structure and low cost is selected. In addition to the special requirements for the selection of the gear pump itself, it should be analyzed from the internal structure of the pump body. The most noteworthy is the unloading groove structure designed to alleviate the phenomenon of trapped oil, and the role of the structure is not only reflected in this point. Many scholars have conducted research on the mechanism of its unloading effect and structural design and improvement.

In addition to the functional analysis and innovative design of the unloading groove, scholars have also developed and refined analysis methods for the flow field in the gear pump, including interpretation and prediction of the flow phenomenon, the proposal and application of more accurate flow field models, and related programs.

[Wei *et al.* \(2021\)](#) designed a trapezoidal unloading groove with larger unloading groove area, more compact structure and easy processing, and proved its efficiency in reducing the trapped oil pressure to alleviate the trapped oil phenomenon and its effects on reducing the flow pulsation at the outlet. [Liu *et al.* \(2020\)](#) proposed a comprehensive design method for a gear pump unloading groove. Based on the numerical simulation of the internal flow field, the designed unloading groove was simulated and analyzed. [Li and Sun \(2012, 2019\)](#) found that the same unloading groove spacing under small side clearance could still be used under large side clearance, and proposed a “large-small-large” H-type side clearance structure on the non-working surface of the driven gear. [Yang *et al.* \(2020\)](#) found that the unloading groove can effectively reduce the pump cavitation phenomenon, and the ability to reduce the pump cavitation phenomenon and oil trapping phenomenon from Torque type–Involute type–Shaped gradually increases, but the volumetric efficiency and machinability gradually decreases. In addition, the most important weakness of these pumps is the severe radial leakage at high pressures. [Sedri and Riasi \(2019\)](#) introduced a new decompression groove on gears that eliminates high-pressure pulsation and abrupt cavitation during gear meshing without increasing radial leakage. [Gao *et al.* \(2015\)](#) applied the meshing tooth width of variable displacement external gear pumps equation, proposing an optimized scheme of opening a wedge-shaped unloading slot at the upper end of the pump-driven gear piston, which effectively reduced the pressure fluctuation in the trapped oil region.

Moreover, most of the literature has been devoted to revealing phenomena of the internal flow field, and exploring the means to demonstrate these. [Romanenko *et al.* \(2022\)](#) demonstrated through

visual analysis that all characteristic positions of the gear are essentially similar in terms of flow and vortex formation, and that flow phenomena in a single meshing cycle can represent the entire gear pump. The positions of the gear teeth with maximum and minimum flow field pressure are also determined. The Standard $k-\epsilon$ RANS model constants are calibrated for the spreading rate of jets in fully developed regions, and do not possess enough freedom to calibrate itself for nonhomogeneous, anisotropic regions of the flow domain ([Zaheer and Masud 2018](#)). [Antoniak and Stryczek \(2018\)](#) proposed a visualization study method which has been used to study flow processes and phenomena in the external gear pump. Findings from the research enabled a detailed description of the flow process, namely of the transporting of the working fluid through the pump, in each of the typical zones of the pump. A characteristic feature of the process is the occurrence of various cavitation phenomena, which made it possible to identify the critical areas of the pump. [Corvaglia *et al.* \(2021\)](#) proposed a new application of three-dimensional model in unsteady flow algorithm. The computational fluid dynamics model is developed in Simerics MP, considering the radial clearance and the change of the tooth side clearance with the change of the shaft angle, and finally has been preliminarily verified in terms of conveying pressure pulsation. [Marinero *et al.* \(2021\)](#) presented an innovative solution to minimize noise emission, acting on the flow ripple, in a prototype external gear pump. The hydraulic model is based on a lumped parameter method using a control volume approach. And Alternative Capacitive Volumes works by controlling and uniformizing the reverse flow, performing a consistent reduction of flow non-uniformity amplitude. [Abdellah *et al.* \(2020\)](#) considered that, the presence of the vortices at the inlet and the outlet strangles the flow. Insertion of a fillet at the inlet and the outlet improves the flow and increases the mass flow of the pump. [Sanchugov and Rekadze \(2022\)](#) presented a new method for analyzing the operation of volumetric pumps. The method is based on wave theory, the method of hydrodynamic analogies and the impedance method, where the pump is considered according to the model in lumped parameters. And the high degree of coincidence of the results confirms that the external gear pump should be considered according to the equivalent source of flow fluctuations model. To address the comparative advantages of gear pump design in terms of compactness or energy performance. [Ransegnola *et al.* \(2019\)](#) developed a program for virtual design optimization of external gear pump, where genetic algorithms can be improved from generation to generation until the optimal design set is determined. A wear degradation state identification method of gear pump based on flow field analysis was proposed by [Guo *et al.* \(2020\)](#). The simulation results show that the instantaneous flow of gear pump decreases with the increase of pressure difference, while the fluctuation amplitude and non-uniformity coefficient of flow increase with the increase of pressure difference. It is proved that the increase of outlet pressure is an important factor causing the internal flow field disorder and pump

body wear of gear pump. Bilalov and Smetannikov (2020) chose the immersed entity method to model the moving boundary. The homogeneous two-phase flow model is used to describe the flow of viscous incompressible fluid with cavitation. It is found that the formation of cavitation region is presented in the form of graphical function dependence and contour map at high speed.

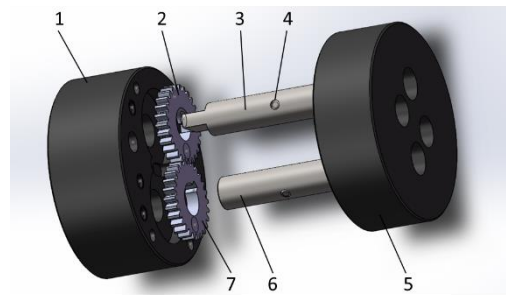
Summarizing the state of research into the unloading groove structure of the gear pump, the spacing of the unloading groove is generally limited to the conventional range, and a number of new designs have made no breakthrough in the spacing. Nowadays, with the continuous improvement of machining accuracy, the applicability of the conventional unloading groove design method to the high-precision gear pump has been reduced. For the high-precision gear pump, it is urgent to further reduce the influence of the unloading groove spacing on the performance of the gear pump. In the numerical simulation, a set of methods with high accuracy and applicability have not yet been formed, including the selection of CFD model and parameter selection. Finally, existing research has failed to apply the quantitative and visual analysis of the unloading groove spacing on the characteristics of multiple flow fields in micro-flow and micro-volume gear pumps. Therefore, this paper explores the influence of unloading groove spacing on multi-flow field performance index and provides an optimization basis according to the actual needs of the project.

2. CALCULATION MODEL AND EXPERIMENTAL VERIFICATION

2.1 Physical Model and Structural Parameters

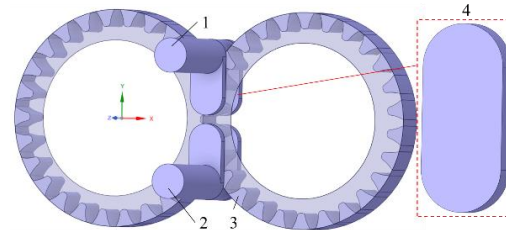
In order to meet the requirements of bidirectional oil supply, small displacement transportation and micro structure size, the gear pump studied in this paper has the following characteristics: large number of teeth, small modulus, high speed, simple and symmetrical structure, no pressure compensation structure such as floating side plate, pump body completely immersed in oil, low oil pollution.

The pump body structure consists of a pair of short-



1-Lower shell; 2-Driving gear; 3- Driving gear shaft; 4-Cylindrical pin; 5-Upper shell; 6- Driven gear shaft; 7-Drive gear

Fig. 1. Bidirectional gear pump structure.



1-Oil absorption area; 2-Oil discharge area; 3-Gear area; 4-Unloading groove area

Fig. 2. Fluid computational domain extraction.

tooth involute gears with identical geometric parameters, upper and lower shells, cylindrical pins, and long and short gear shafts. The known gear pump parameters are shown in Table 1, and the three-dimensional model is established according to the relevant parameters. The SolidWorks exploded structure diagram is shown in Fig. 1.

In Spaceclaim, the closed surface method was used to extract the computational domain of the internal flow field of the model, and then this domain was divided into multiple parts as shown in Fig. 2 (e.g., the oil absorption area, the oil discharge area, the gear area, and the unloading groove area). The focal object of this paper is a circular arc unloading groove. Compared with rectangular and special-shaped unloading grooves, the structure is simple, easy to process, and the unloading effect is better.

2.2 Mesh Division and Independence Verification

After a large number of experiments on various meshing methods, it was found that for ensuring both grid quality and calculation accuracy, sweep meshing was the only meshing type that could best meet the Fluent dynamic grid simulation calculation, which is based on the two-dimensional mechanical rotation motion of the gear pump (Bie de *et al.* 2021). Independence verification is carried out from the direction of mesh size refinement. Three groups of control experiments are set up. It is necessary to ensure that the number of meshes increases in all directions and the mesh topology does not change. The specific mesh division is shown in Table 2:

Table 1 Gear pump parameters

Parameter	Value
z	26
$m(\text{mm})$	0.9
$d_a(\text{mm})$	25.05
$d_f(\text{mm})$	21.42
$B(\text{mm})$	4
$\alpha (^{\circ})$	20
$d_t(\text{mm})$	2
$h_a(\text{mm})$	0.015
$h_r(\text{mm})$	0.02

Table 2 Control groups mesh division

Group	Nodes	Elements	Skewness
1	876462	1656483	0.1231
2	225881	451052	0.1311
3	107281	210796	0.1522

The evaluation criterion for mesh quality is the degree of distortion, or skewness, which ranges from 0 to 1, with values closer to 0 indicating better quality. From Table 2, it can be seen that the finer the mesh division is, the less corresponding distortion, and the higher the mesh quality. From the number of nodes and units, the three sets of data increase in a certain proportion. As revealed by Fluent simulation, the similarity of the three groups of flow curves was high, and the average flow rate was 0.01407 kg/s (see Fig. 3). According to the average value and the flow pulsation rate of the experimental results, the corresponding curve is fitted. The comparison shows that the simulation curve is in the allowable range of error, which can prove the validity of the simulation and the mesh independence. However, in the case of calculating the same step size, the time used in group 1 was 5 times that of group 3. Therefore, in order to reduce the computing time and computing resources, the grid division method of group 3 was selected for subsequent numerical simulation, as shown in Fig. 4.

2.3 Hydrodynamical Model

Viscous model

Because the flow inside the gear pump, especially at the radial clearance, encompasses not only the differential pressure flow, but also the strong shear flow, the RNG k-ε turbulence model was selected to

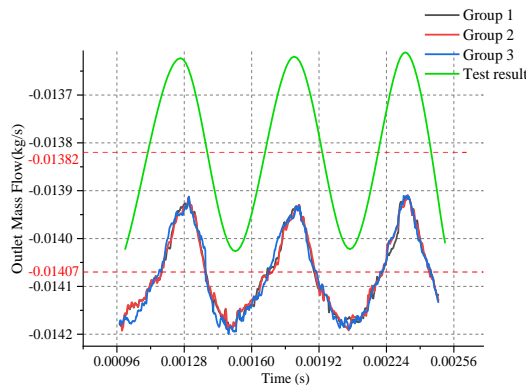


Fig. 3. Outlet flow comparison.

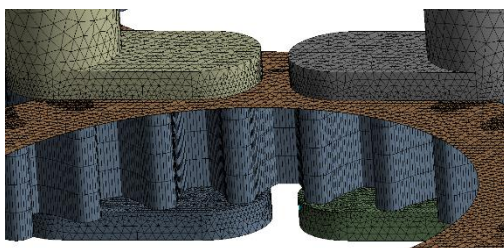


Fig. 4. Mesh division of Group 3.

adapt to the complex internal flow field. The turbulent viscosity was modified and the accuracy effectively improved by an analytical formula considering the low Reynolds number flow viscosity.

Cavitation model

In order to simulate the influence of gas on the internal flow field, the gas-liquid multiphase flow model was selected, and the material properties of oil, oil vapor, and air were set. The mass exchange between the gas phase and the liquid phase is described by the gas transport equation as follows.

$$\frac{\partial}{\partial t} (\varphi_g \rho_v) + \nabla \cdot (\varphi_g \rho_v \vec{u}_v) = R_e - R_c \quad (1)$$

The generation and collapse of bubbles during cavitation is described by the Reyleigh-Plesset equation (Liu 2016).

The Zwart-Gerber-Belamri cavitation model uses a number of adjustable parameters such as void fraction and initial bubble radius to predict the gas volume fraction in the flow field more accurately. So, we adopted this as the cavitation model. According to the test site environment, the air separation pressure and saturated vapor pressure should be set to 4000 Pa and 1500 Pa, respectively.

2.4 Dynamic Mesh

The dynamic characteristics of the gear pump cannot be obtained through static simulation alone. At this time, 2.5D dynamic grid simulation technology is needed. The connection line between the grid nodes is approximated as a spring by using the spring smoothing method, and the position of each node is obtained by calculating the force balance equation between the nodes.

$$\vec{F}_i = \sum_j^{n_j} k_{ij} (\Delta \vec{x}_j - \Delta \vec{x}_i) \quad (2)$$

At the same time, the grid reconstruction method is used to limit the maximum size of the grid motion to 1.8 L_{max} and the minimum size to 0.3 L_{min}. Spring constant factor set to 0.2. The boundary point relaxation factor is 0.9. The boundary condition is set to 0.24 MPa pressure boundary inlet and 14 MPa pressure boundary outlet. Two gear surfaces are set to rigid motion, both end faces are set to Deforming on the plane, the form of motion is controlled by the UDF, using the DEFINE_CG_MOTION macro to define the axial speed 2200r/min. Pressure velocity coupling uses coupled algorithm; The discrete schemes of turbulent kinetic energy and turbulent dissipation rate are second order upwind scheme.

2.5 Test Verification

In order to ensure the reliability of the numerical simulation results, test verification was carried out in collaboration with the relevant partners. As shown in Fig. 5, the electromagnetic flowmeter is connected to the outlet end of the gear pump, and the oil

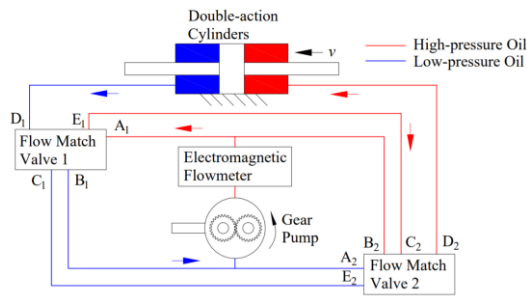


Fig. 5. Test schematic diagram.

movement in the pipeline is converted into induced electromotive force by using the principle of electromagnetic induction, so as to monitor the outlet flow of the pump.

According to the above numerical simulation principle, the initial model is established and simulated. The simulation results of gear pump outlet flow are compared with the experimental results. Under no-load condition, the simulation result is 18.25 ml/s, the test result is 18.18 ml/s, and the error is 0.39 %. Under the working pressure, the simulation result is 16.34 ml/s, the test result is 16.06 ml/s, and the error is 1.74 %. All of them are within the allowable range of error, which proves that the existing model has a good performance in the simulation analysis and prediction of gear pump flow field, and can basically meet the simulation requirements.

3. NUMERICAL SIMULATION OF GEAR PUMP FLOW FIELD

3.1 Design Principle of Unloading Groove

The design principle of the conventional unloading groove is shown in Fig.6. The symmetrical position of the two meshing points B1 and B2 on the node P

is defined as the critical position. The contour lines of the unloading grooves at both ends need to pass through the meshing points respectively to prevent the two unloading grooves from being connected through the side gap during the oil trapping process, so that the oil suction chamber and the oil discharge chamber are connected (Liu *et al.* 2022). In this paper, the unloading groove spacing of the model under this design principle is 2.0 mm.

3.2 Simulation Result Analysis of Unloading Area

Due to the larger trapped oil pressure, the internal leakage will increase, the oil temperature will increase, and the pump body will be impacted greatly, causing vibration and noise (Zhao and Vacca 2019). Therefore, the simulation results of the initial model are processed, and the instantaneous pressure cloud diagram is shown in Fig. 7. The change law of the action position of the unloading groove is observed. The wireframe in the figure represents the trapped oil area, and the dot represents the meshing point.

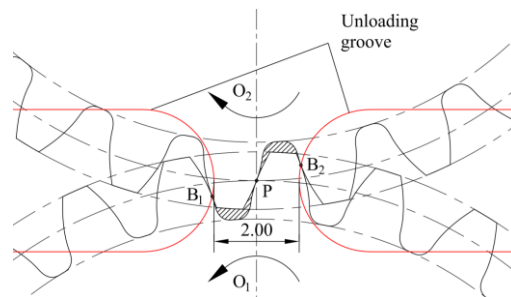


Fig. 6. Conventional design spacing.

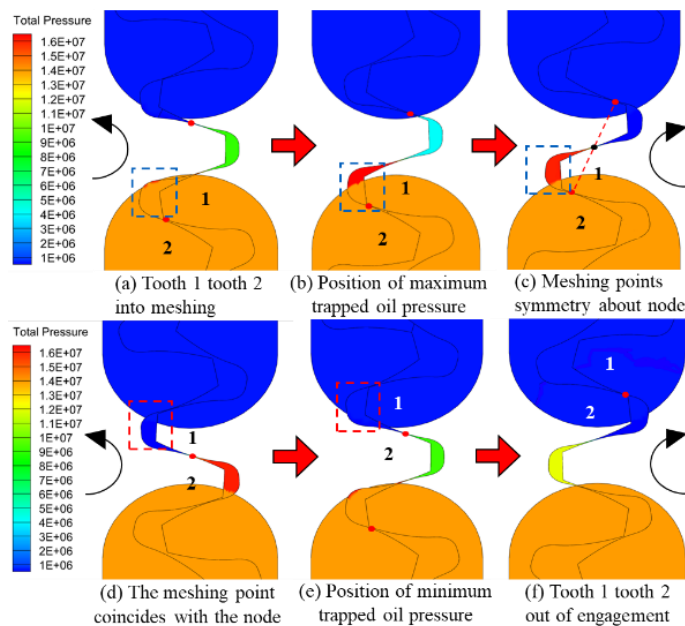


Fig. 7. Instantaneous pressure contour of meshing part.

It can be seen from Fig.7 that as the gear rotates, when the trapped oil part gradually breaks away from the range of the unloading groove, the unloading area gradually becomes smaller. At the position where trapped oil pressure is maximum, trapped oil volume is not completely out of the unloading groove coverage, and has not yet reached the minimum volume. This indicates that the pressure release under the action of the unloading groove at this position is balanced with the pressure increase caused by the compression of the trapped oil volume. The existence of the unloading groove increases the flow area between the two teeth, so that the trapped oil pressure has begun to decline when the trapped oil volume has not reached the minimum value. In this process, the maximum value of trapped oil pressure and its change rule have an important influence on the stability of flow field.

3.3 Simulation Result Analysis of Oil Replenishment Area

In the gear pump flow field, the phenomenon of cavitation manifests mainly as bubbles: those formed by gas dissolved in the oil when the oil pressure is lower than the air separation pressure; and those formed by vaporization of the oil surface molecules when the oil pressure is lower than the saturated vapor pressure. The bubble content in the initial state is set to 0, and the initial bubble radius is set to 1e-05 m according to the cavitation model used in 2.3. The bubble formation rate was 1, the condensation coefficient 0.01, the air density 1.225 kg/m³, and the absolute viscosity 1.79e-05 Pa·s. The density of oil vapor was 1.95 kg/m³, with absolute viscosity of 7e-06 Pa·s. Therefore, as can be seen in Fig. 8, with rotation of the gear, bubbles are continuously generated in the oil filling area under the action of the pressure field, which occurs in the form of high-speed swirl or even jet, and the measurement parameters of the bubble amount are expressed by the gas volume fraction.

The gas volume in the flow field includes air and oil vapor. The results show that the air part accounts for about 99.2 %, which indicates that the oil pressure in the oil replenishment area is not easy to reach below the saturated vapor pressure. Compared with the bubbles formed by air precipitation, the oil vaporization process has less influence on cavitation. As shown in Fig. 8, the gear is rotated from the left position to the right position, the trapped oil volume becomes larger and larger, the oil pressure is released

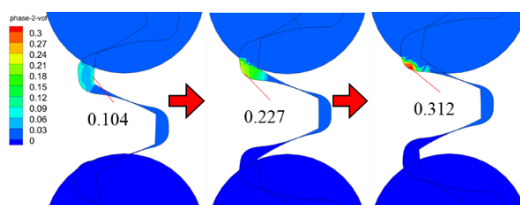


Fig. 8. Gas volume distribution contour of meshing part.

and quickly reduced to below the air separation pressure, the trapped oil volume enters the part of the unloading groove area, the oil is replenished, and almost no cavitation occurs, and the trapped oil volume that does not enter the unloading groove area will precipitate a large amount of gas under the action of pressure to supplement the expanding volume. In this process, the increase of gas volume fraction from 0.104 to 0.312 is continuous in one direction, and the maximum value can be used as a key index of the gas output in this process. The consequence of gas production is that when these bubbles are brought to the high-pressure zone by the oil, the bubbles are compressed and ruptured to produce a considerable impact force, which will cause serious cavitation corrosion on the tooth surface, cause vibration and noise, and greatly shorten the gear life. Therefore, the ability to reduce the volume of gas in the flow field is also one of the important indicators to measure the effect of the unloading groove. (Zhou *at al.* 2020).

4. ANALYSIS OF FLOW FIELD CHARACTERISTICS OF GEAR PUMP

In order to further analyze the influence of the spacing of unloading grooves on flow field characteristics, eight sets of parameters were set with the conventional design spacing as reference: 0.5, 0.75, 1.0, 1.25, 1.5, 1.75, 2.0, 2.5 mm to form a control experiment.

4.1 Analysis of Influence of Unloading Groove spacing on Trapped Oil Pressure

Figure 9 shows the variation curves of trapped oil pressure in unloading area of eight groups of numerical simulation results in the same time period. Each curve is fitted by 38 sampling points with sampling interval of 2E-5s. The x axis coordinate corresponding to the initial change position of each curve is the time when the unloading zone begins to leave the unloading groove range, and the y axis coordinate is the working load of 14 MPa.

It can be seen from Fig. 9 that the process of increasing trapped oil pressure is also the process of decreasing unloading amount. When the peak value

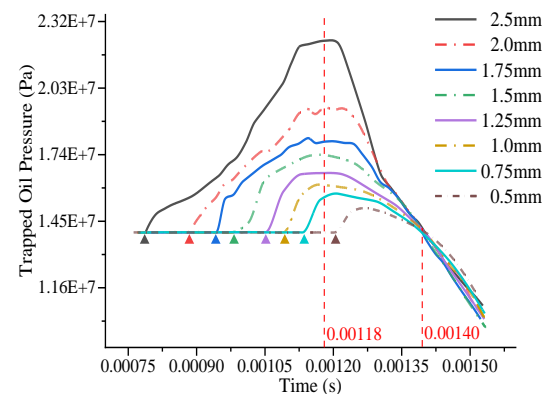


Fig. 9. Trapped oil pressure curve at different spacings.

is reached, the pressure increase caused by trapped oil volume compression is balanced against the pressure release caused by unloading groove action. From the analysis of the x -axis direction, except for the large coverage area of the 0.5 mm spacing unloading groove, the pressure change time was late, and the maximum trapped oil pressure of the remaining curves was concentrated at about 0.00118s. Since the initial state of the gears in the eight test groups was the same, the simultaneous position of the gears was also the same, so it can be shown that the position of the maximum trapped oil volume depends on the compression change of the trapped oil volume, rather than the unloading groove effect. Moreover, the trapped oil pressure changes regularly in the process of each curve dropping from the beginning to 0.00141 s to 14 MPa working load.

From analyzing the y -axis direction, when the unloading slot spacing was greater than 1.75 mm, the pressure rise was relatively slow but the duration of trapped oil phenomenon was longer; when the unloading groove spacing was below 1.5 mm, the pressure rose more rapidly, and the change rate in the front of the curve was close. In addition, it can be seen from Fig. 8 that when the trapped oil pressure reaches the peak value, it will remain for a period of time, then accelerate the decline, and the smaller the unloading groove spacing, the slower the decline. Our analysis revealed that the peak retention is due to the fact that the trapped oil volume at the gear position is near the limit value, which belongs to the transition stage, and the change rate is very small, so the stable stage will appear around the peak. On the whole, the smaller the unloading groove spacing, the more stable the curve changes, the shorter the high-pressure duration, and the less damage to the gear pump.

The maximum trapped oil pressure value at each spacing is extracted and analyzed as shown in Fig. 10. The trend of the curve is nearly linear. The maximum trapped oil pressure is 15.0 MPa at 0.5 mm spacing and 22.9 MPa at 2.5 mm spacing, which is 7.46 % and 63.43 % higher than the working pressure, respectively. This shows that reducing the spacing of unloading slots can effectively alleviate the surge of trapped oil pressure, thereby reducing the harm of vibration and noise caused by trapped oil phenomenon, and has a positive effect on the flow field performance.

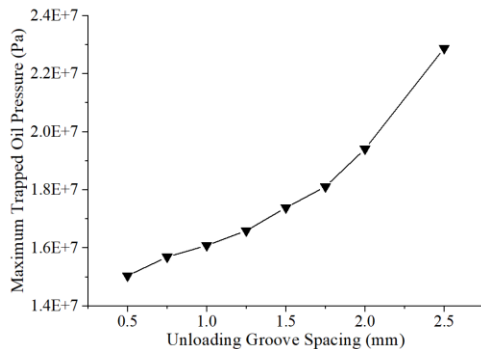


Fig. 10. Maximum trapped oil pressure curve with spacings.

4.2 Analysis of Influence of Unloading Groove spacing on Flow Quality

The theoretical derivation and calculation of the instantaneous flow rate of the gear pump outlet were carried out. This analysis shows that the maximum instantaneous flow rate occurs when the meshing point coincides with the node, and the minimum instantaneous flow rate occurs at the symmetrical position of the two meshing points about the node. The average flow rate of the outlet is:

$$\bar{Q} = \omega B(r_a^2 - r_k^2 - \frac{1}{12}t_j^2) \quad (3)$$

The flow curve is pulsating, and the flow pulsation coefficient is:

$$\delta = \frac{Q_{max} - Q_{min}}{Q} = \frac{3\pi^2 \cos^2 \alpha}{12(Z + h_a)h_a - \pi^2 \cos^2 \alpha} \times 100\% \quad (4)$$

The average flow rate is 18.32 ml/s, the mass flow rate is 0.01534 kg/s, and the flow pulsation coefficient is 2.86 %. This provides a theoretical reference for the numerical simulation results (Rituraj and Andrea 2021).

The instantaneous flow of the simulation results under three pulsation periods is analyzed. Figure 11 and Fig. 12 use the same x -axis and y -axis coordinate scales. Figure 11 is the flow curve under the spacing of 1.0, 1.75 and 2.5 mm unloading grooves. It can be seen from the figure that with the decrease of the spacing within a certain range, the amount of oil sent back to the oil absorption chamber through the excessive compression of the trapped oil volume

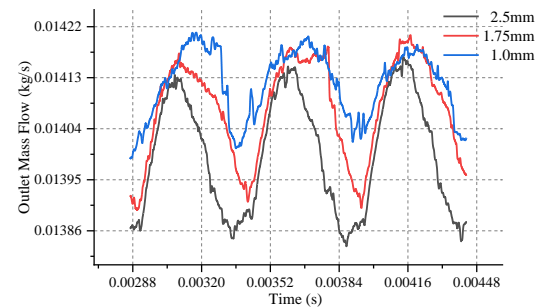


Fig. 11. Flow curve under 1.0, 1.75, 2.5 mm groove spacings.

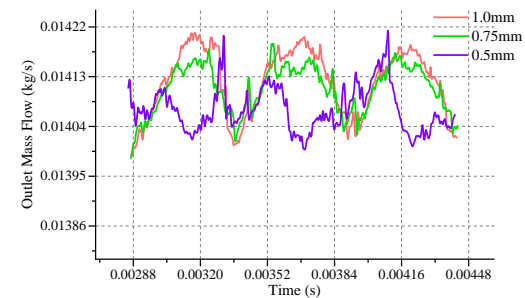


Fig. 12. Flow curve under 0.5, 0.75, 1.0 mm groove spacings.

decreases, the flow curve moves up as a whole, and the flow pulsation coefficient gradually decreases.

As shown in Fig. 12, when the unloading groove spacing is further reduced from 1.0 mm, the flow value shows a downward trend as a whole, and when the spacing is 0.5 mm, the curve pulsation is not significant, and the curve in each time period is no longer regular. Analysis shows that due to the unloading groove spacing is too small, when the gear rotation to the trapped oil pressure is lower than the working pressure position, under the action of pressure, the high-pressure oil discharge chamber through the trapped oil volume squeezed into the suction chamber, resulting in a decline in the outlet flow. At the same time, the degree of turbulence at the unloading groove increases, and the local eddy current phenomenon increases, resulting in the loss of pulsation characteristics of the flow curve.

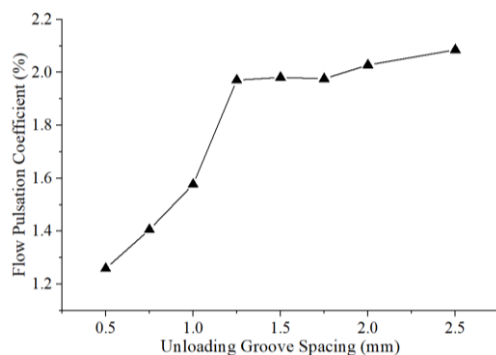


Fig. 13. Flow pulsation coefficient under different unloading groove spacings.

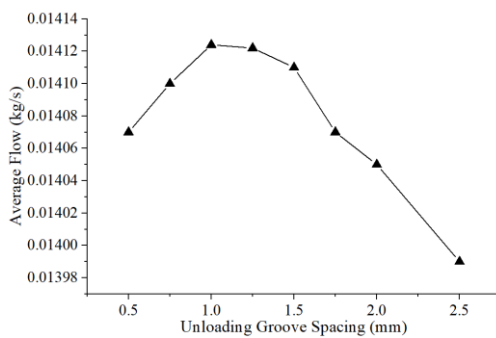


Fig. 14. Average flow under different unloading groove spacings.

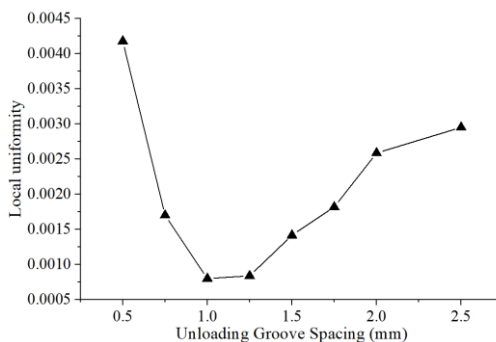


Fig. 15. Local uniformity under different unloading groove spacings

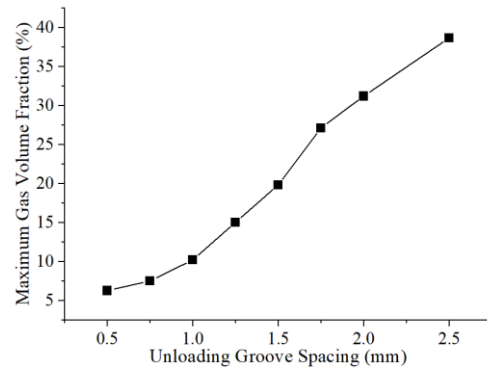


Fig. 16. Curve of maximum gas volume fraction with spacings.

From the perspective of numerical statistics, the flow quality under each spacing is evaluated by flow pulsation coefficient, flow mean and uniformity of concerned parts (Zhang and Jin 2015). The uniformity of the concerned part refers to the variance of the data near the peak of the flow curve divided by the average. It can be seen from Fig.13 to Fig.15 that the flow pulsation coefficient decreases gradually with the decrease of spacing, and the reduction rate becomes faster when the spacing is less than 1.25 mm. The average flow rate increases first and then decreases with the decrease of the spacing. According to the theoretical reference calculation, when the unloading groove spacing is 1.0 to 1.5 mm, the average flow rate is higher than 0.01411 kg/s, which meets the expected requirement of 92 % volumetric efficiency. Also, the uniformity of the concerned parts also shows a more uniform trend with the decrease of the spacing from 2.5 to 1.0 mm. However, when the spacing continues to decrease, the irregularity of the curve leads to the deterioration of the flow uniformity and the decrease of the flow stability.

4.3 Analysis of the Influence of Unloading Groove Spacing on Cavitation Phenomenon

From the variation of the maximum gas volume fraction shown in Fig. 16, it can be seen that as the distance between the unloading slots decreases, the curve changes nearly linearly, the amount of gas generated in the flow field also decreases, the cavitation phenomenon weakens, and the harm caused by cavitation also decreases. This is because when the unloading groove spacing decreases, the range of the unloading groove covering the trapped oil volume in the oil replenishment area increases, and the closed volume that is completely separated from the unloading groove during the rotation of the gear decreases, so the amount of oil below the air separation pressure and saturated vapor pressure is reduced.

5. DETERMINATION OF EVALUATION INDEX SYSTEM

Since the unloading slot spacing has an important influence on the multi-flow field characteristic index,

it is necessary to clear the relationship between the single factor and each index. The actual demand of engineering is that the accuracy of hydraulic system affected by flow quality is more important than the performance of gear pump affected by cavitation. In this paper, based on the combination of qualitative and quantitative analysis, the analytic hierarchy process (Chen 2021) is used to clarify the goal of improving the flow field performance under structural improvement, so as to establish a mathematical model, perform dimensionless processing on each index and calculate the relative weight ω . The dimensionless processing results are as follows:

Table 3 Dimensionless treatment of each index

Spacing (mm)	P	δ	Q_a	F	T
2.5	1	1	-0.9905	0.7057	1
2.0	0.8486	0.9727	-0.9948	0.6184	0.8072
1.75	0.7917	0.9477	-0.9962	0.4349	0.7016
1.5	0.7601	0.9501	-0.9990	0.3386	0.5131
1.25	0.7254	0.9453	-0.9999	0.2007	0.3888
1.0	0.7033	0.7564	-1	0.1914	0.2642
0.75	0.6859	0.6743	-0.9983	0.4067	0.1947
0.5	0.6576	0.6038	-0.9962	1	0.1627

Get the initial matrix:

$$\begin{matrix} P \\ \delta \\ Q_a \\ F \\ T \end{matrix} \begin{pmatrix} 1 & 0.5 & 0.2 & 0.25 & 2 \\ 2 & 1 & 0.25 & 0.5 & 1 \\ 5 & 4 & 1 & 0.5 & 2 \\ 4 & 2 & 2 & 1 & 5 \\ 0.5 & 1 & 0.5 & 0.2 & 1 \end{pmatrix}$$

Matrix normalization conversion:

$$\begin{pmatrix} 0.0800 & 0.0588 & 0.0506 & 0.1020 & 0.1818 \\ 0.1600 & 0.1176 & 0.0633 & 0.2041 & 0.0909 \\ 0.4000 & 0.4706 & 0.2532 & 0.2041 & 0.1818 \\ 0.3200 & 0.2353 & 0.5063 & 0.4082 & 0.4545 \\ 0.0400 & 0.1176 & 0.1266 & 0.0816 & 0.0909 \end{pmatrix}$$

Easy target matrix:

$$\omega (0.0947 \quad 0.1272 \quad 0.3019 \quad 0.3848 \quad 0.0914)$$

The rationality of the weights obtained by the consistency and randomness test matrix is tested by the test formula:

$$CR = \frac{CI}{RI} \tag{5}$$

where CI represents the consistency index of judgment matrix, $CI = \frac{\lambda_{max} - n}{n - 1}$, λ_{max} is the maximum eigenvalue of the matrix, $\lambda = \sum_{i=1}^n \frac{(AW)_i}{nW_i}$, RI represents the average

Table 4 Evaluation results of each spacin

Spacing (mm)	0.5	0.75	1.0	1.25
Value	0.2380	0.0236	-0.0414	-0.0002
Spacing (mm)	1.5	1.75	2.0	2.5
Value	0.0684	0.1262	0.2154	0.2858

randomness index of the judgment matrix. When the index number n is 5, RI is 1.12.

When the CR value is less than 0.1, the matrix conclusion is established, and the calculation result CR is $0.08351 < 0.1$, which meets the requirements. The evaluation index system is:

$$Y = 0.0947P + 0.1272\delta + 0.3019Q_a + 0.3848F + 0.0914T$$

The evaluation results of the spacing of each unloading groove are shown in Table 4. Smaller evaluation values indicate better flow field performance.

As evaluated by this system, an unloading groove spacing of 1.0 mm meets flow field requirements of both high flow accuracy and low vibration noise. Compared with principal design spacing of 2.0 mm, the maximum trapped oil pressure was 1.609 MPa, 17.13 % lower than 1.941 MPa. The flow pulsation coefficient is reduced from 2.028 % to 1.577 %. the flow average is increased to meet the volume efficiency expectation; flow local uniformity increased by 68.76 %; the maximum gas volume fraction decreased by 20 % from 31.219 % to 10.219 %. The performance of each flow field has been greatly improved, which is a better result after measuring the weight of each index. This provides a proof and analysis for the influence of unloading groove spacing on the flow field characteristics, and has a certain guiding role in selecting the appropriate spacing.

6. CONCLUSION

(1) For the gear pump structure studied in this paper, the pressure cloud diagram of the trapped oil phenomenon and the gas volume fraction of the cavitation phenomenon were obtained by numerical simulation. The flow field during the gear rotation was visually analyzed. The more clear and specific change law of the trapped oil pressure, the gas precipitation process and gas volume fraction change in the flow field are obtained.

(2) Our analysis of the numerical simulation results, revealed that the maximum trapped oil pressure and the maximum gas volume fraction change linearly with distance. Reducing the distance between unloading grooves can effectively alleviate the trapped oil phenomenon and reduce the degree of cavitation. At the same time, its impact on flow quality is more complex, flow pulsation coefficient changes rapidly when the unloading slot spacing is less than 1.25 mm, the minimum can reach 1.259 %; the average flow rate increases first and then

decreases, reaching the peak at 1.0 mm spacing. When the spacing is less than 1.0 mm, the local uniformity becomes worse, the flow curve loses the pulsation characteristics, and the flow stability decreases. Overall, break the unloading slot spacing of the conventional design range, to further improve the performance of the gear pump has a higher upgrade.

(3) The analytic hierarchy process was used to analyze the dimensionless weight of each evaluation index, concluding that the unloading effect under the spacing of 1.0 mm unloading groove is better. Compared with the original design spacing, the maximum trapped oil pressure is reduced by 17.13 %, the flow pulsation coefficient is reduced from 2.028 % to 1.577 %, which meets the volume efficiency expectation, the flow uniformity is improved by 68.76 %, and the maximum gas volume fraction is reduced by 20 %. It provides an optimization basis for improving the flow accuracy of gear pump and reducing low pulsation noise.

ACKNOWLEDGEMENTS

This work received funding from the National Natural Science Foundation of China (No. 51975092).

REFERENCES

- Abdellah El-Hadj, A. and Abd S. Z. B. Rahim (2020). Optimization of an External Gear Pump using Response Surface Method. *Journal of Mechanics* 36(4), 567-575.
- Antoniak, P. and J. Stryczek (2018). Visualization study of the flow processes and phenomena in the external gear pump. *Archives of Civil and Mechanical Engineering* 18(4).
- Bie de, V. G., M. A. Hulsen and P. D. Anderson (2021). Finite element modeling of a viscous fluid flowing through an external gear pump. *Macromolecular Theory and Simulations* 30(1), 2000060.
- Bilalov, P. A. and O. Y. Smetannikov (2020). Numerical investigation of fluid dynamics phenomena in external gear pump. *Computational Continuum Mechanics* 13(4), 471-480.
- Chen, P. Y. (2021). Complementarity of indicators in multi-index comprehensive evaluation method. *Statistics and Decision-Making* 37(22), 22-26.
- Corvaglia, A., A. Ferrari, M. Rundo and O. Vento (2021). Three-dimensional model of an external gear pump with an experimental evaluation of the flow ripple. *Proceedings of the Institution of Mechanical Engineers, Part C: Journal of Mechanical Engineering Science* 235(6), 1097-1105.
- Gao, J. H., Y. S. Wang, L. H. Zhao, H. Guo and J. G. Li (2015). Unloading groove optimization and the inner flow-field simulation analysis of the variable displacement external gear pump. *Journal of Mechanical Transmission* 39(5), 133-137.
- Guo, R., Y. Li, Y. Shi, H. Li, J. Zhao and D. Gao (2020). Research on identification method of wear degradation of external gear pump based on flow field analysis. *Sensors* 20(14), 4058.
- Li, Y. L. and F. C. Sun (2012). Quantitative analysis of the relationship between gear pump tooth side clearance and unloading slot spacing. *Journal of Agricultural Engineering* 28(22), 63-68.
- Li, Y. L. and F. C. Sun (2019). Study on H-type side clearance structure of gear pair trapped oil unloading for pump. *Journal of Engineering Design* 26(01), 15-19.
- Liu, H. M. Pan, J. Fu, H. Li and R. Cao (2022). A new type unloading groove design and simulation for engine fuel gear pump. In *2022 13th International Conference on Mechanical and Aerospace Engineering (ICMAE)*.
- Liu, Y. (2016). *CFD-Based Three-Dimensional Numerical Calculation Method of High-Pressure Internal Gear Pump and Its Unbalanced Radial Force*. Ph. D. thesis, Zhejiang University, Zhejiang, China.
- Liu, Z. L., Y. F. Hu, L. Cui, W. F. Zhu and J. Li (2020). Design of gear pump unloading groove and simulation of its internal flow field characteristics. *Hydraulic and Pneumatic* 09, 100-107.
- Marinero, G., E. Frosina and A. Senatore (2021). A numerical analysis of an innovative flow ripple reduction method for external gear pumps. *Energies* 14(2), 471.
- Ransegnola, T., X. Zhao and A. Vacca (2019). A comparison of helical and spur external gear machines for fluid power applications: Design and optimization, *Mechanism and Machine Theory* 142.
- Rituraj, R. and V. Andrea (2021). Investigation of flow through curved constrictions for leakage flow modelling in hydraulic gear pumps. *Mechanical Systems and Signal Processing* 153.
- Romanenko, I., Y. Martseniuk and O. Bilohub (2022). Modeling the meshing procedure of the external gear fuel pump using a CFD tool. *Computation* 10(7), 114.
- Sanchugov, V. and P. Rekadze (2022). New method to determine the dynamic fluid flow rate at the gear pump outlet. *Energies* 15(9), 3451.
- Sedri, F. and A. Riassi (2019). Investigation of leakage within an external gear pump with new decompression slots: numerical and experimental study. *Journal of the Brazilian Society of Mechanical Sciences and Engineering* 41(5).
- Wei, L. J., T. Li, L. F. Lu, Y. Qiang and X. M. Luo

- (2021). Research on the influence of trapezoidal unloading groove on trapped oil pressure and flow pulsation of external gear pump. *Hydraulic and Pneumatic* 45(03), 62-69.
- Yang, G. L., W. Y. Wang, J. H. Bai, J. Jin, M. M. Zhang and F. T. Huang (2020). Cavitation characteristics of external gear pump under different unloading grooves. *Manufacturing Technology and Machine Tools* 09, 106-111.
- Zaheer, Q. and J. Masud, (2018). Comparison of flow field simulation of liquid ejector pump using standard k- ϵ and embedded les turbulence modelling techniques. *Journal of Applied Fluid Mechanics* 11(2), 385-395.
- Zhang, Y. X. and J. Jin (2015). Instantaneous flow and flow pulsation suppression of gear pump. *Hydraulic and Pneumatic* 03, 46-49.
- Zhao, X. and A. Vacca (2019). Theoretical investigation into the ripple source of external gear pumps. *Energies* 12(3), 535.
- Zhou, J., S. Yuan and C. Jing (2020). Research on flow characteristics of gear pump considering cavitation effect. *Army Journal* 41(1), 189-195.